The Journal of Chemical Physics

RESEARCH ARTICLE | AUGUST 31 2017

# Contact angles from Young's equation in molecular dynamics simulations

Hao Jiang ; Florian Müller-Plathe; Athanassios Z. Panagiotopoulos

Check for updates

*J. Chem. Phys.* 147, 084708 (2017)
https://doi.org/10.1063/1.4994088
CHORUS

View Online
Export Citation
CrossMark

09 January 2024 14:51:36

AIP Publishing

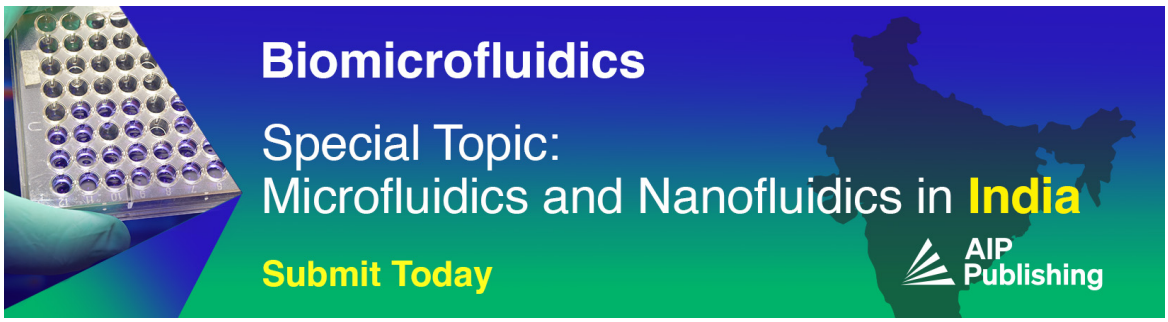

# Contact angles from Young's equation in molecular dynamics simulations

Hao Jiang,[1] Florian Müller-Plathe,[1,2] and Athanassios Z. Panagiotopoulos[1,a)]
[1]*Department of Chemical and Biological Engineering, Princeton University, Princeton, New Jersey 08544, USA*
[2]*Technische Universität Darmstadt, Eduard-Zintl-Institut für Anorganische und Physikalische Chemie, Alarich-Weiss-Str. 8, D-64287 Darmstadt, Germany*

(Received 3 July 2017; accepted 14 August 2017; published online 31 August 2017)

We propose a method to calculate the equilibrium contact angle of heterogeneous 3-phase solid/fluid/fluid systems using molecular dynamics simulations. The proposed method, which combines the phantom-wall method [F. Leroy and F. Müller-Plathe, J. Chem. Phys. **133**, 044110 (2010)] and Bennett's acceptance ratio approach [C. H. Bennett, J. Comput. Phys. **22**, 245 (1976)], is able to calculate the solid/fluid surface tension relative to the solid surface energy. The calculated relative surface tensions can then be used in Young's equation to estimate the equilibrium contact angle. A fluid droplet is not needed for the proposed method, in contrast to the situation for direct simulations of contact angles. In addition, while prior free-energy based methods for contact angles mainly focused on the wetting of fluids in coexistence with their vapor on solid surfaces, the proposed approach was designed to study the contact angles of fluid mixtures on solid surfaces above the fluid saturation pressures. Using the proposed approach, the contact angles of binary Lennard-Jones fluid mixtures on a non-polar solid substrate were calculated at various interaction parameters and the contact angle of water in equilibrium with $CO_2$ on a hydrophilic polar silica surface was obtained. For both non-polar and polar systems, the calculated contact angles from the proposed method were in agreement with those obtained from the geometry of a cylindrical droplet. The computational cost of the proposed method was found to be comparable to that of simulations that use fluid droplets, but the new method provides a way to calculate the contact angle directly from Young's equation without ambiguity. *Published by AIP Publishing.* [http://dx.doi.org/10.1063/1.4994088]

09 January 2024 14:51:36

## I. INTRODUCTION

Wettability is of great interest to various scientific and industrial applications, such as surface chemistry, coating, or oil recovery.[1] Wettability describes the balance of interfacial interactions for a solid/fluid system. From a thermodynamic point of view, such balance can be expressed in Young's equation

$$\cos\theta = \frac{\gamma_{sf_2} - \gamma_{sf_1}}{\gamma_{f_{1,2}}}, \tag{1}$$

where $\theta$ is the equilibrium (or Young's) contact angle, $\gamma$ are interfacial (or surface) tensions, $s$ refers to the solid phase, and $f_1$ and $f_2$ refer to the two fluid phases. For a pure fluid in equilibrium with its vapor, $f_1$ and $f_2$ refer to the liquid and vapor phases, respectively. Although the fluid/fluid (or vapor/liquid) surface tension can be measured with satisfactory accuracy in experiments, the solid/fluid surface tension cannot be measured directly; therefore, the wettability of a heterogeneous solid/fluid system is usually described by the contact angle, which is the angle formed between the solid/fluid (or solid/liquid) interface and the fluid/fluid (or vapor/liquid) interface. A common approach to measure contact angles in experiments is the sessile droplet method: a fluid droplet is placed on a solid substrate with the droplet geometry captured by a camera, and the contact angle can be obtained from the geometry of the droplet.

Molecular dynamics (MD) and Monte Carlo (MC) simulations are useful tools for microscopic modeling of wetting phenomena for solid/fluid systems. There have been numerous studies reporting contact angles for a variety of systems including Lennard-Jones (LJ),[2–5] water/graphite (graphene),[6–9] water/$CO_2$(or oil)/minerals,[10–14] etc. In most such studies, the calculation of the contact angle follows an approach similar to that of experimental measurements: the initial configuration is constructed by placing a fluid droplet above a solid substrate, and after the system is equilibrated, the contact angle is estimated from the shape of the fluid droplet. Although the implementation of such a simulation is relatively straightforward, there are several issues that require attention. In an experiment, the fluid droplet has macroscopic dimensions (typically mm and above), while the size of the fluid droplet used in MD or MC simulations is on the order of nm. It is well known that the contact angle of a spherical nano-scale droplet is additionally affected by the curvature of the 3-phase contact line and the vapor-liquid interface.[15] To address this problem, periodic cylindrical droplets, which have an infinite radius for the 3-phase contact line, can be used in simulations.[16] However, Scocchi *et al.*[17] found that the contact angle of a cylindrical droplet on a hydrophobic surface is dependent on the droplet radius. Therefore, in order to minimize the system size effect in the contact angle calculation, cylindrical

a)Author to whom correspondence should be addressed: azp@princeton.edu.

droplets with a large radius have to be used, which makes simulations computationally expensive. In addition, the contact angle cannot be unambiguously estimated from the geometry of a fluid droplet, as there is some subjectivity involved in identifying the precise location of the interface between the droplet and its surrounding fluid and solid. Such ambiguity introduces uncertainty to the estimation of contact angles, especially for highly hydrophilic surfaces. When the contact angle is small (<20°), estimation of contact angles from the geometry of nano-droplets in simulations becomes increasingly difficult.

These difficulties in contact angle calculations are rooted in the use of actual droplets in simulations. It is therefore highly desirable to develop methods to obtain surface free energies of solid/fluid systems, from which contact angles can be obtained directly from Young's equation, without having a fluid droplet explicitly present in a simulated system. Several algorithms have been developed towards this goal. Gloor *et al.*[18] proposed the test-area method, which can be used to obtain the surface tension for fluid/fluid interfaces as well as for solid/fluid interfaces. This method was used to calculate the surface tensions between an NaCl crystal, aqueous NaCl solution, and air; the resulting surface tensions were in good agreement with experimental data.[19] Leroy and Müller-Plathe[20,21] developed a method to calculate the solid/fluid surface free energy relative to the solid surface energy. In this method, the actual solid/fluid interface is reversibly transformed to a structureless repulsive wall (termed a "phantom wall"). The free-energy change associated with the transition is obtained using thermodynamic integration. The phantom-wall method has been applied to the wetting properties of a LJ system and water on graphene.[7] Later, Leroy and Müller-Plathe developed the dry-surface method to determine the work of adhesion of solid/fluid interfaces. The contact angle can be deduced from the work of adhesion using the Young-Dupré equation.[22] In the dry-surface approach, the solid/fluid work of adhesion is calculated from a thermodynamic integration process by reversibly turning off the attractive part of the solid/fluid interaction. The dry-surface approach was applied to calculate the work of adhesion for water on non-polar gold surfaces, water on graphene surfaces,[23] as well as water on polar $MoS_2$ surfaces.[24] In the dry-surface approach, the surface tension between the liquid and a repulsive wall was assumed to be equal to the vapor/liquid surface tension; however, such assumption may not necessarily be valid above the liquid saturation pressure.[22] Errington and co-workers[25–28] developed the interface potential approach to compute the contact angle of water on non-polar surfaces. The interface potential approach uses Monte Carlo simulation in the grand canonical ensemble to calculate the surface excess free energy associated with the growth of a fluid film on a surface, i.e., the work of adhesion. There are two variants of interface potential: the spreading potential that grows a liquid film near a solid surface, therefore suitable for a system having strong solid/fluid interaction, and the drying potential that grows a vapor film near a solid surface, suitable for a system with weak solid/fluid interaction. In the grand canonical simulations, the liquid is in equilibrium with its saturated vapor, and the interface potential approach has not been extended to systems with two fluid components at high pressure. Recently, Kanduc and Netz[29,30] developed a thermodynamic integration method to calculate the surface free energy of water on flat hydrophilic polar surfaces. It was found that the interface potential exhibits a minimum when a finite number of water vapor molecules are absorbed on the polar surface, which indicates that a thin water film is thermodynamically stable on a polar surface. Kanduc and Netz drew the important conclusion that presence of such a thin fluid film lowers the surface free energy, consequently increasing the contact angle of a hydrophilic surface. This effect is most pronounced for strongly hydrophilic surfaces near a wetting transition. Kanduc and Netz did not investigate mixed fluids at high pressures, and it is not straightforward to apply their approach to estimate film thickness for systems above the vapor-phase saturation pressure.

In the present work, we focus on wetting phenomena of binary fluid mixtures at pressures above the saturation vapor pressure of each fluid component, instead of dealing with a pure liquid in equilibrium with its vapor on a solid surface. Wetting of multiphase systems is of particular interest to geochemistry, oil recovery, and geological $CO_2$ sequestration.[31] Fluid flow in underground porous formations is significantly affected by fluid/rock wettability. Here, we develop a surface-free-energy based molecular dynamics algorithm, which allows us to obtain the contact angle of fluid mixtures on solids directly from Young's equation, without resorting to an explicit nano-scale fluid droplet. It is worth mentioning that the validity of Young's equation at the nanoscale remains an open question. In an early MD simulation, Saville[32] studied surface tensions and contact angles for a system consisting of a Lennard-Jones fluid and a continuum representation of a LJ solid. It was found that Young's equation yielded contact angles inconsistent with those obtained directly from the density distribution of a microscopic droplet. However, a few recent molecular dynamics and Monte Carlo simulation studies[33–35] have demonstrated the validity of Young's equation at the molecular level. The proposed algorithm combines the phantom-wall method[20] and Bennett's acceptance ratio method[36] to estimate the solid/fluid surface tension relative to the solid/vacuum surface tension, hereafter referred to as relative solid/fluid surface tension. We first apply the proposed algorithm to calculate the contact angle of binary LJ fluid mixtures on a non-polar LJ solid. In order to validate the proposed method, we obtain the contact angle for several LJ systems and compare the results with those obtained from conventional droplet simulations. We also study the contact angle of a water/$CO_2$ mixture on a hydrophilic, polar silica surface, a system relevant for $CO_2$ geological sequestration.[37]

The structure of this paper is as follows: in Sec. II, we describe our method for the calculation of relative surface tensions. In Sec. III, the details of simulations and molecular models are given. We compare calculated contact angles using the proposed method with those from droplet simulations in Sec. IV. A comparison of computational cost between simulations using the proposed method and those using the fluid droplet is also given in Sec. IV. Finally, the conclusions from the present work are summarized in Sec. V.

09 January 2024 14:51:36

## II. METHODS

The proposed method is used to calculate the contact angle of two immiscible fluids (termed $f_1$ and $f_2$) on a solid substrate ($s$). According to Eq. (1), the contact angle ($\theta$) can be calculated once the surface tensions between the solid and the two fluids ($\gamma_{sf_1}$ and $\gamma_{sf_2}$) and the surface tension between the two fluids ($\gamma_{f_{1,2}}$) are known. The methods to calculate the fluid/fluid surface tension are well established, and this property is usually obtained through the anisotropy of the pressure tensor elements ($P_{xx}$, $P_{yy}$, and $P_{zz}$) in MD simulations,[38]

$$\gamma_{f_{1,2}} = \frac{1}{2} L_z \Big( P_{zz} - 0.5(P_{xx} + P_{yy}) \Big), \tag{2}$$

where $L_z$ is the length of the simulation box in the direction perpendicular to the fluid/fluid interface. Unfortunately, the solid/fluid surface tension generally cannot be obtained using Eq. (2) due to the presence of internal stress in the solid phase. Among several techniques that have been proposed to calculate the solid/fluid surface tension,[39–43] the cleaving-wall method[40] is probably the most widely used. However, this method requires careful handling of boundary conditions, and its implementation for solids with complex internal structure, e.g., clay minerals, is not straightforward. In order to estimate the equilibrium contact angle from Eq. (1), the difference of surface tensions between the solid and two fluids, i.e., the relative surface tensions, is needed, rather than the absolute value of the solid/fluid surface tension.

The phantom-wall method[20] can be used to estimate the relative solid/liquid surface tension. Details of the method can be found in the original publications[20,21] and are only briefly described here. In this approach, the actual solid surface is reversibly turned into a purely repulsive and structureless "phantom wall" using thermodynamic integration. In a MD simulation, the phantom wall is modeled as an atomic interaction center, and it is connected to one of the central atoms in the solid via a harmonic spring. The phantom wall interacts only with fluid atoms through a repulsive [e.g., Weeks-Chandler-Andersen (WCA)] potential along the direction normal to the interface; there is no interaction between the phantom wall and solid atoms. At the beginning of the thermodynamic integration calculation, the phantom wall is embedded in the solid phase and it cannot interact with fluid atoms since the distance between it and the fluid molecules is beyond the cutoff distance of the repulsive potential. The phantom wall is then slowly pushed out of the solid by increasing the equilibrium length of the harmonic spring. With the phantom wall moving away from the center of the solid, it starts interacting with the fluid, and the fluid is "lifted" away from the solid surface until the solid/fluid interaction decays to a negligible value. Implementation of the phantom-wall method is illustrated in Fig. 1. The free-energy difference ($G_{\mathrm{AB}}$) between the initial (A) and final (B) states shown in Fig. 1, or equivalently, the work required to lift the fluid away from the solid, can be calculated by numerically integrating the spring force ($f_{sp}$) over the equilibrium spring length ($Z_0$) along a reversible path,[20]

$$G_{\mathrm{AB}} = \int_{Z_A}^{Z_B} f_{sp} dZ_0. \tag{3}$$

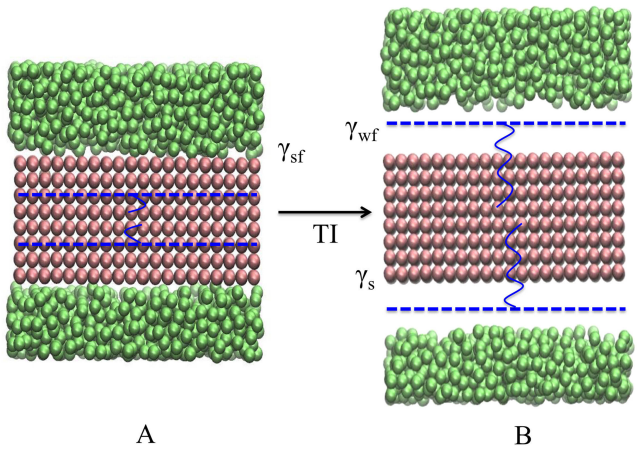


FIG. 1. Schematic representation of the phantom-wall method. Phantom walls are shown as blue dashed lines and connected to the center solid atoms with harmonic springs (blue wavy lines), respectively. Two phantom walls are used due to the periodic boundary conditions. The solid and liquid phases are presented as the red and green atoms, respectively.

The free-energy difference ($G_{\mathrm{AB}}$) between the initial and final states is related to the solid/fluid surface tension ($\gamma_{sf}$) as

$$G_{\mathrm{AB}}/2A = \gamma_s + \gamma_{wf} - \gamma_{sf} + P\Delta V/2A, \tag{4}$$

where $A$ is the area of the solid/fluid interface, $\gamma_{wf}$ is the phantom wall/fluid surface tension, $\gamma_s$ is the solid/vacuum surface tension (or the solid surface energy). Simulations are performed in the $NPzT$ ensemble with the solid/fluid interface parallel to the $xy$ plane, and $\Delta V$ is the system volume change during the thermodynamic integration. The phantom-wall method gives the relative solid/fluid surface tension ($\gamma'_{sf} = \gamma_s - \gamma_{sf}$), provided the phantom wall/fluid surface tension ($\gamma_{wf}$) can be obtained.

Equation (4) for the solid ($s$) and two fluid phases ($f_1$ and $f_2$) can be written as

$$\gamma'_{sf_1} = (G_{\mathrm{AB},sf_1} - P\Delta V_1)/2A = \gamma_s + \gamma_{wf1} - \gamma_{sf_1}, \tag{5}$$

$$\gamma'_{sf_2} = (G_{\mathrm{AB},sf_2} - P\Delta V_2)/2A = \gamma_s + \gamma_{wf2} - \gamma_{sf_2}, \tag{6}$$

and with Young's equation [Eq. (1)], the equilibrium contact angle ($\theta$) is calculated as

$$\cos\theta = \frac{(\gamma'_{sf_1} - \gamma'_{sf_2}) - (\gamma_{wf1} - \gamma_{wf2})}{\gamma_{f12}}. \tag{7}$$

The fluid/fluid ($\gamma_{f12}$) and phantom wall/fluid ($\gamma_{wf1}$ and $\gamma_{wf2}$) surface tensions can then be calculated using Eq. (2) without the presence of the solid phase. In practice, we performed five sets of independent simulations to estimate each quantity in Eq. (7): two sets of simulations were conducted to calculate $\gamma'_{sf_1}$ and $\gamma'_{sf_2}$ using the phantom wall as well as the acceptance ratio method (described below); another three sets of simulations were conducted to obtain the fluid/fluid and phantom wall/fluid surface tensions using Eq. (2).

In order to calculate reliably the free-energy difference between the initial (A) and final (B) states, it is essential that the thermodynamic integration is performed along a reversible path. However, such a path may be inaccessible for systems with strong solid/fluid attractions. Fluid atoms may form a film (layering) on a highly hydrophilic solid substrate; when

09 January 2024 14:51:36

the phantom wall moves close to the solid/fluid interface, the repulsive phantom wall/fluid potential strongly perturbs the fluid layer at the interface, which may induce an abrupt change of structure (possibly a phase transition) for the fluid and make the integration path non-reversible. It was reported that the phantom wall method becomes less stable with a strong solid/fluid interaction.[22] In order to overcome this problem, we incorporated Bennett's acceptance ratio (BAR) method[36] into the calculation of relative solid/fluid surface tensions. In particular, we introduced a scaling parameter $\lambda$ to adjust the interaction between the fluid and solid,

$$U_{sf}(\lambda) = \sum_{is=1}^{N_s} \sum_{if=1}^{N_f} u_{is,if}(r, \lambda), \tag{8}$$

where the parameter $\lambda$ ranges from 1.0 to $\lambda_0$, with $\lambda = 1.0$ corresponding to the actual solid/fluid interaction of interest. $\lambda_0$ is an arbitrary value that makes the fluid only weakly attracting the solid. Fluid/fluid and solid/solid interactions are not affected by $\lambda$, so the free-energy difference between two neighbouring intermediate states ($\lambda_k$ and $\lambda_{k+1}$) corresponds to the change of surface free energy and can be estimated from Eqs. (9) and (10),[36]

$$\frac{n_k}{n_{k+1}} = \frac{\left\langle f\left(\beta U_{sf}(\lambda_k) - \beta U_{sf}(\lambda_{k+1}) + C_k\right)\right\rangle_{k+1}}{\left\langle f\left(\beta U_{sf}(\lambda_{i+1}) - \beta U_{sf}(\lambda_k) - C_k\right)\right\rangle_{k}}, \tag{9}$$

where $n_k$ is the number of statistical independent samples at the state $k$ and $f(x) = 1/(1 + e^x)$. The free-energy difference between the solid/fluid interface of interest and the interface with weak solid/fluid interaction is calculated by summing the free-energy differences at all intermediate states,

$$G_{\mathrm{BAR}} = \sum_{k=1(\lambda=1.0)}^{k=m(\lambda=\lambda_0)} \frac{1}{\beta}(C_k + ln\frac{n_k}{n_{k+1}}). \tag{10}$$

With the BAR method, we effectively turn the actual solid/fluid interface ($\lambda = 1.0$) to a hydrophobic interface with reduced solid/fluid attraction ($\lambda = \lambda_0$). For the interface with weak solid/fluid attractions, the relative solid/fluid surface tension can be obtained using the phantom wall method [Eq. (3)] without experiencing a discontinuous structure change for the fluid near the interface. The relative solid/fluid surface tensions ($\gamma'_{sf}$) in Eqs. (5) and (6) are the sum of surface free energies (per unit area) obtained with the phantom-wall [Eq. (3)] and BAR [Eq. (10)] methods.

## III. MOLECULAR MODELS AND SIMULATION DETAILS

We studied the contact angle of heterogeneous LJ solid/fluid(1)/fluid(2) systems. For the non-polar LJ systems, the interaction between two particles, ($i$) and ($j$), is given as

$$u(r_{ij}) = 4\epsilon_{ij}[(\frac{\sigma_{ij}}{r_{ij}})^{12} - (\frac{\sigma_{ij}}{r_{ij}})^{6}], \tag{11}$$

where the energy ($\epsilon$) and size ($\sigma$) parameters for solid atoms were 32 and 1.2 (in LJ reduced units), respectively. The use of a large energy parameter for the solid atoms ensured the stability of the solid crystal structure. The size parameters of fluid 1 ($\sigma_{f1}$) and 2 ($\sigma_{f2}$) were both set to 1.0, and the size parameters for cross interaction between the solid and fluids ($\sigma_{sf_1}$ and $\sigma_{sf_2}$) were set to 1.1. The energy ($\epsilon_{f1,2}$) and size ($\sigma_{f1,2}$) parameters for the LJ potential between two fluids are 0.1 and 1.2, respectively. We explored a wide range of energy parameters for solid/fluid ($\epsilon_{sf_1}$ and $\epsilon_{sf_2}$) interactions, and these parameters are given in Table I. The cutoff distance for the LJ potential was 3.75 and the LJ potential was switched to zero at 4.0. Two phantom walls were used in simulations due to the periodic boundary conditions. The phantom walls interacted with fluids through a purely repulsive WCA potential with both its energy and size parameters set to 1.0, and the phantom walls were connected to the central solid atoms by a harmonic spring with force constant set to 1000. The simulations for both the BAR and phantom-wall methods were conducted in the $NPzT$ ensemble with periodic boundaries in all dimensions. A well-equilibrated solid substrate was put in contact with the fluid, forming a flat interface parallel to the $xy$ plane. The solid substrate had a face-centred-cubic structure (100), and the base system contained 1600 solid and 2000 fluid atoms. We also simulated a system that had 6400 solid and 8000 fluid atoms, and the free energies obtained agreed with those from the base system. Simulations were carried out at $T^* = 0.9$ and $P_z^* = 0.1$ and 0.5. The temperature was controlled using the Langevin thermostat[44] with a time constant of 1.0, and the pressure was controlled using the Parrinello-Rahman barostat[45] with a time constant of 2.0. For simulations using both the phantom wall and acceptance ratio methods, the system was equilibrated for $1 \times 10^6$ MD steps, followed by a production period of $4 \times 10^6$ steps. The time step was set to 0.002.

We turned the solid/fluid interface of interest to an interface where the solid only weakly attracts the fluid using the BAR method. In order to achieve this, the energy parameter ($\epsilon_{k,sf}$) of solid/fluid LJ interaction was multiplied by $\lambda$ at each state ($k$). At the final state, we chose $\lambda$ that makes $\epsilon_{k,sf}$ equal to 0.1, which is small enough to make the solid/fluid attraction weak. With $\epsilon_{end,sf} = 0.1$, the phantom-wall method was

TABLE I. Contact angles of a LJ fluid on a non-polar LJ solid substrate with different interaction parameters at $T^* = 0.9$.

| | | | | |
|---|---|---|---|---|
| $P_z^* = 0.1$, $\epsilon_{f1} = 1.1$, $\epsilon_{f2} = 0.2$ | | | | |
| $\epsilon_{s,f1}$ | 0.8 | 0.8 | 0.5 | |
| $\epsilon_{s,f2}$ | 0.1 | 0.4 | 0.1 | |
| $\theta$ (PW + BAR) | 62(1) | 71(1) | 114(1) | |
| $\theta$ (droplet) | 62(1) | 70(1) | 113(1) | |
| $P_z^* = 0.1$, $\epsilon_{f1} = 1.1$, $\epsilon_{f2} = 0.9$ | | | | |
| $\epsilon_{s,f1}$ | 0.5 | 0.8 | 0.9 | 0.9 |
| $\epsilon_{s,f2}$ | 0.2 | 0.2 | 0.2 | 0.1 |
| $\theta$ (PW + BAR) | 85(1) | 53(1) | 34(4) | 26(4) |
| $\theta$ (droplet) | 87(1) | 52(1) | 38(3) | 33(3) |
| $P_z^* = 0.5$, $\epsilon_{f1} = 1.1$, $\epsilon_{f2} = 0.2$ | | | | |
| $\epsilon_{s,f1}$ | 0.9 | 0.9 | 0.9 | 0.9 |
| $\epsilon_{s,f2}$ | 0.1 | 0.3 | 0.5 | 0.6 |
| $\theta$ (PW + BAR) | 42(3) | 60(1) | 77(1) | 84(1) |
| $\theta$ (droplet) | 45(4) | 62(2) | 74(1) | 86(1) |

09 January 2024 14:51:36

used to calculate the relative solid/fluid surface tensions ($\gamma'_{sf_1}$ and $\gamma'_{sf_2}$), which were combined with the surface free energy obtained using the BAR method to estimate the contact angle using Eqs. (5)–(7).

For the calculation of phantom wall/fluid surface tensions ($\gamma_{wf1}$ and $\gamma_{wf2}$), one phantom-wall atom and 2000 fluid atoms were placed in a rectangular box ($L_x = L_y = 10$, $L_x < L_z$), forming an interface parallel to the $xy$ plane, and the system was equilibrated for $5 \times 10^6$ steps, followed by a production period of $15 \times 10^6$ steps in the $NP_zT$ ensemble. The pressure tensor elements obtained in the simulations were used in Eq. (2) to calculate the surface tension. The surface tension between two fluids ($\gamma_{f_{1,2}}$) was obtained in a similar manner: 1000 atoms of fluid 1 and 1000 atoms of fluid 2 were placed in a rectangular box and the pressure tensor elements were averaged over a $15 \times 10^6$ steps production run after the system was equilibrated for $5 \times 10^6$ steps.

In order to validate the proposed method for contact angle calculation, we also performed MD simulations to estimate contact angles from the geometry of cylindrical fluid droplets on the solid substrate. The cylindrical droplet, which was periodic in the $y$ dimension, was made from the fluid (fluid 1) that has a stronger interaction with the solid. The fluid droplet contained 5000 atoms and the surrounding fluid (fluid 2) contained 20 000 atoms. The solid substrate was made of 4200 atoms with its $x$ dimension ($L_x = 65.01$) larger than its $y$ dimension ($L_y = 18.57$). The simulations were conducted in the $NP_zT$ ensemble, and the Langevin thermostat[44] and Parrinello-Rahman barostat[45] were used to regulate the system temperature and pressure ($P_z$). The system was equilibrated for $5 \times 10^6$ steps, followed by a production period of $3 \times 10^6$ steps, and snapshots were output every 50 000 steps for the analysis of the contact angle. The geometry of the droplet was determined from the interface between the droplet and its surrounding fluid, and the interface was defined as the position where the mole fraction of fluid 1 (fluid in droplet) is equal to 0.5, and the contact angle was calculated as

$$\theta = \arcsin\left(\frac{2hb}{h^2 + b^2}\right), \tag{12}$$

where $h$ and $b$ are the height and base radius of the fluid droplet, respectively. A figure showing the mole fraction distribution map used for contact angle estimation is given in the supplementary material. In order to make sure the contact angle obtained from the geometry of the droplet was not strongly affected by the droplet radius, we also conducted a MD simulation with a droplet made from 7000 fluid 1 atoms (in equilibrium with 20 000 fluid 2 atoms on a solid substrate made of 7800 atoms), and the contact angles obtained from the larger system agreed with that obtained from a droplet of 5000 atoms, which indicated that a droplet of 5000 atoms was large enough to make system size effects negligible.

For the polar water/$CO_2$/silica system, the INTERFACE force field[46] was used to represent the silica Q2 surface, which had a surface silanol density of 9.4 $nm^{-2}$. Since our goal here is to demonstrate the methodology for contact angle calculation, we chose to use the simple SPC/E water[47] and the semiflexible EPM2 $CO_2$[48] force fields rather than more accurate, but computationally slower, molecular models that are now available.[49,50] The INTERFACE, SPC/E, and EPM2 models use Lennard-Jones potential and point charges to represent the intermolecular interactions,

$$U_{ij}(r_{ij}) = \frac{1}{4\pi\epsilon_0}\frac{q_i q_j}{r_{ij}} + 4\epsilon_{ij}\left[\left(\frac{\sigma_{ij}}{r_{ij}}\right)^{12} - \left(\frac{\sigma_{ij}}{r_{ij}}\right)^{6}\right]. \tag{13}$$

The detailed force field parameters can be found in the supplementary material. The cross interactions for LJ potential between water, $CO_2$, and silica atoms follow the Lorentz-Berthelot combining rule.

The silica Q2 surface strongly interacts with water by forming hydrogen bonds, and the phantom wall may induce a structure change (or phase transition) for water near the silica surface, similar to the LJ system with strong solid/fluid attractions. It is therefore necessary to reversibly turn the hydrophilic silica Q2 surface to a hydrophobic one using the BAR method. In the simulations for BAR calculations, we introduced the scaling parameter $\lambda$ into the combining rule for the cross interaction between water (oxygen atoms of water) and oxygen atoms of the silanol group,

$$\sigma_{Ow,Os} = \lambda\left(\frac{\sigma_{Ow} + \sigma_{Os}}{2}\right), \tag{14}$$

where $\lambda$ = [1.0, 1.001, 1.005, 1.01, 1.02, …, 1.1, 1.12, …, 1.2] with $\lambda = 1.0$ corresponding to the actual silica/water interface of interest. The free-energy difference between states with $\lambda = 1.0$ and $\lambda = 1.2$ was obtained using the BAR method, and the phantom-wall method was used to calculate the relative surface tension for the silica/water interface with weak interaction (at $\lambda = 1.2$). For the phantom-wall method, the averaged spring forces ($fsp$) were obtained at 19 different values of spring equilibrium length to perform numerical integration according to Eq. (3). The equilibrium spring length was varied from 7 Å to 24 Å for the silica/water system and from 7 Å to 18 Å for the silica/$CO_2$ system. The choice of equilibrium spring length for the thermodynamic integration can be found in the supplementary material. For the silica/$CO_2$ interface, the phantom-wall method can be applied without preceding it by the BAR method since the silica/$CO_2$ interaction is relatively weak.

For the water/$CO_2$/silica system, the simulations were performed at 318 K and 145 bars, similar to a prior study by Chen *et al.*[14] For the phantom wall and BAR calculations, the simulations were performed in the $NP_zT$ ensemble using the Langevin thermostat[44] and Parrinello-Rahman barostat.[45] The system was equilibrated for 0.5 ns followed by a production period of 1.0 ns with a time step of 1.0 fs at each stage. The cutoff distance for the LJ potential and real-space part of electrostatic interactions was 1 nm, and the reciprocal part of the electrostatic interactions was handled by the particle mesh Ewald summation.[51] The phantom walls interacted with water and $CO_2$ through a WCA potential with its energy and size parameters set to 0.1 kcal/mol and 0.15 nm, respectively. The force constant for the harmonic spring was 3000 kcal/mol/nm. The shake algorithm[53] was used to constrain the internal geometry of water and the bond length of $CO_2$ molecules. The phantom wall/water, phantom wall/$CO_2$, and water/$CO_2$ surface tensions were obtained from pressure tensor elements using Eq. (2). For the calculation of phantom wall/water (or

09 January 2024 14:51:36

$CO_2$) surface tensions, 2000 water (or $CO_2$) molecules were placed into a rectangular box ($L_x = L_y = 2.8$ nm) with 1 phantom wall atom. The simulations were performed in the $NP_zT$ ensemble using the Langevin thermostat[44] (time constant 100) and Parrinello-Rahman barostat with time constant 500.[45] The LJ and real-space electrostatic interactions were truncated at 1.35 nm, beyond which the interaction is negligible. The system was equilibrated for 5 ns followed by a production run of 15 ns with a time step of 1 fs. Similarly, the water/$CO_2$ surface tension was calculated with 2000 water and 2000 $CO_2$ molecules using pressure tensor elements in a rectangular box.

In order to validate the proposed method for the polar water/$CO_2$/silica system, the contact angle of a cylindrical water droplet in equilibrium with $CO_2$ on the silica Q2 surface was also obtained from its geometry in a MD simulation (Fig. 2). In the direct simulation, the solid silica had a dimension of 20.8 nm × 3.39 nm × 1.88 nm. It contained 11 088 atoms, and it was first equilibrated at the target temperature and pressure. 2000 water molecules, which were initially arranged into a cylindrical droplet above the solid substrate, and 4000 $CO_2$ molecules were used in the simulation. For the silica solid, the bulk oxygen and silicon atoms were held fixed during the simulation, while the silanol oxygen and hydrogen atoms were able to move. The temperature of the system was controlled with the Langevin thermostat,[44] while the pressure of the system was controlled by placing a piston, which was made from a layer of FCC structured atoms, above the fluid phases. The piston atoms interacted with water and $CO_2$ through a purely repulsive WCA potential, and an external force ($=P \times A$) corresponding to the system pressure was applied to drive the piston atoms towards the fluid. The system was periodic only in $x$ and $y$ dimensions. The cutoff distance for the LJ potential and real-space part of electrostatic interactions was 1.2 nm, and the reciprocal part of the electrostatic interactions was handled by the particle mesh Ewald summation[51] modified by Yeh and Berkowitz to handle the non-periodic condition in the $z$ dimension.[52] The system was equilibrated for 6 ns followed by a production period of 3 ns. During the production period, the system configurations were saved every 50 000 steps for the analysis of the contact angle. The contact angle was calculated using Eq. (12), and the droplet dimensions were estimated manually from plots of water molecule mole fraction as did Tenney and Cygan in their calculation of contact angles for the water/$CO_2$/clay system.[13] All MD simulations were performed using LAMMPS[54] with in-house modification to handle the phantom-wall method. The statistical uncertainties were estimated from the block averages by dividing the production period into 10 blocks.

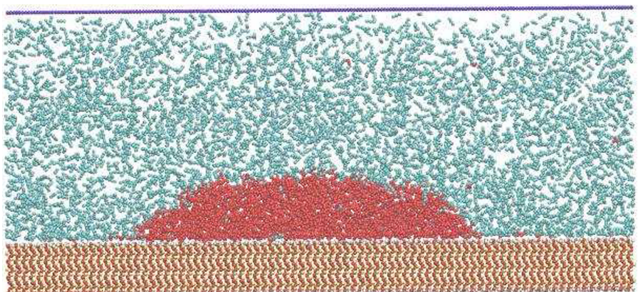

FIG. 2. Snapshot from a MD simulation for the calculation of contact angles using a cylindrical water droplet in equilibrium with $CO_2$ on a silica Q2 surface. The purple line at the top corresponds to the FCC piston atoms controlling the system pressure.

## IV. RESULTS AND DISCUSSION

The contact angles of binary LJ fluid mixtures on nonpolar LJ solids at various solid/fluid interaction parameters, as well as the contact angle of water in $CO_2$ on the silica Q2 surface, were calculated. The obtained relative solid/fluid surface tensions, phantom wall/fluid and fluid/fluid surface tensions with their associated statistical uncertainties, and examples of mole fraction distribution map are given in the supplementary material.

### A. Lennard-Jones systems

We chose to use the LJ solid/fluid system with $\epsilon_{sf} = 0.9$ and $\sigma_{sf} = 1.1$ to illustrate the necessity of combining the BAR method with the phantom-wall method. Figure 3 shows the spring force ($f_{sp}$) and the length of the simulation box in the $z$ dimension ($L_z$) at different equilibrium lengths ($Z_0$) of the harmonic spring at $T^* = 0.9$ and $P_z^* = 0.1$. As described in Sec. II, the phantom walls were embedded in the solid phase at the beginning of the thermodynamic integration ($Z_0 < 2.5$), and they did not interact with fluid atoms, therefore no spring force acted on them. While the phantom walls were pushed towards the fluid by increasing the equilibrium length of the harmonic spring, they started repelling the fluid, and the spring force as well as the box length ($L_z$) increased. When the phantom wall moved close to the solid/fluid interface (around $Z_0 = 3.8$), the phantom walls strongly disturbed the layers of fluid atoms formed at the solid/fluid interface due to the strong solid/fluid attraction ($\epsilon_{sf} = 0.9$). The strong repulsive interaction between the phantom walls and fluid caused a dramatic change of fluid structure near the solid/fluid interface, which can be

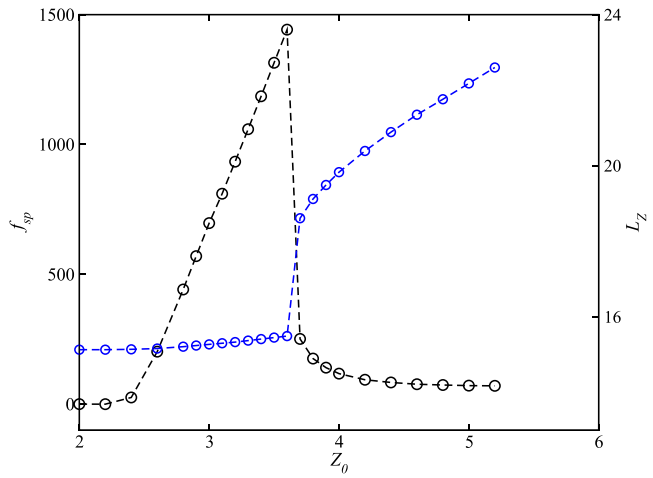


FIG. 3. Spring force ($f_{sp}$, black symbols) and simulation box length ($L_z$, blue symbols) at different spring equilibrium lengths ($Z_0$) for the Lennard-Jones fluid/solid system at $T^* = 0.9$ and $P_z^* = 0.1$ with $\epsilon_{sf} = 0.9$ and $\sigma_{sf} = 1.1$. The dashed lines are a guide to the eye.

09 January 2024 14:51:36

observed by the dramatic increase of box size and the sharp decrease of spring force. This sudden transition precluded us from an accurate calculation of the surface free energy for the system.

The BAR method can be used to overcome this issue. We chose scaling parameters $\lambda$ ($\epsilon_{sf,k} = \lambda\epsilon_{sf}$) equal to 1.0, 8/9, 7/9, . . . , 1/9, so the energy parameters ($\epsilon_{sf,k}$) of the solid/fluid LJ potential were 0.9, 0.8, . . . , 0.1 at each intermediate state ($k$). We then followed Eqs. (9) and (10) to calculate the free-energy difference between the state of interest ($\epsilon_{sf} = 0.9$), i.e., the actual fully interacting surface, and the weakly interacting final state ($\epsilon_{sf,end} = 0.1$). As shown in Fig. 4, the free-energy difference between the state of interest and the final state changes smoothly with $\lambda$, and the dramatic change of box length was not observed, which indicates that the BAR method can be used reliably to turn an interface with strong solid/fluid interaction to an interface with weak interaction without experiencing any significant transition of the fluid structure.

For a system with a weak solid/fluid interaction (e.g., $\epsilon_{sf,end} = 0.1$), the phantom-wall method can be used. As shown in Fig. 5, the spring force ($f_{sp}$) varies smoothly as the phantom wall approached the solid/liquid interface and no sharp increase of box length was observed. The surface free energy was calculated by numerically integrating the spring force ($f_{sp}$) over the spring length ($Z_0$) using the trapezoidal rule.

The contact angles for LJ systems were obtained using the proposed method at various interaction parameters, and these results are given in Table I. As a reference for comparison, the contact angles of a binary LJ fluid mixture on the LJ solid were also estimated from the geometry of cylindrical droplets in MD simulations, and these results are also shown in Table I. The LJ systems studied are at pressures ($P_z^*$) much higher than the saturation pressure of each fluid; fluid 1, which has a stronger interaction with the solid than fluid 2, formed droplets in direct MD simulations. As shown in Table I, the studied LJ

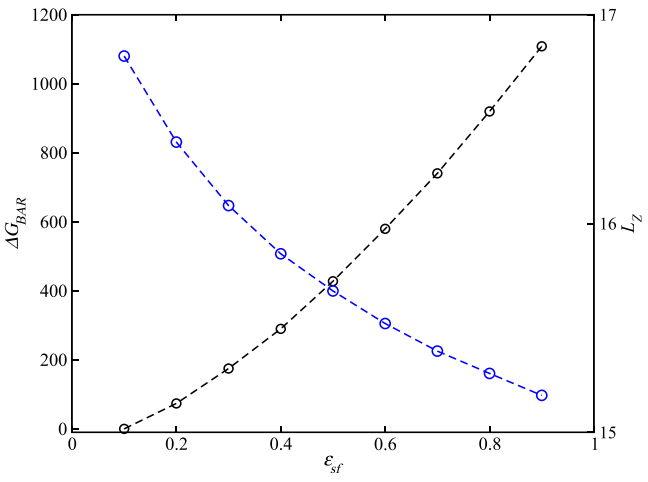


FIG. 4. Gibbs free energy (black symbols) of the state of interest (fully interacting surface $\epsilon_{sf} = 0.9$) and each intermediate state ($\epsilon_{sf,k} = 0.2$-$0.8$) relative to an artificial weakly interacting final state ($\epsilon_{sf,end} = 0.1$) at $T^* = 0.9$ and $P_z^* = 0.1$ for the LJ solid/fluid system. Blue symbols are the simulation box lengths ($L_z$) at each state. The dashed lines are a guide to the eye.

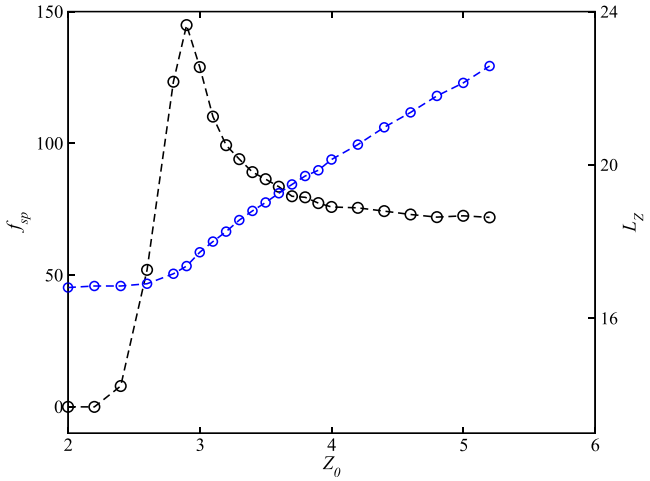


FIG. 5. Spring force ($f_{sp}$, black symbols) and simulation box length ($L_z$, blue symbols) at different spring equilibrium lengths ($Z_0$) for the LJ fluid/solid system at $T^* = 0.9$ and $P_z^* = 0.1$ with $\epsilon_{sf} = 0.1$ and $\sigma_{sf} = 1.1$. The dashed lines are a guide to the eye.

systems have contact angles ranging from 26° to 114°. For the wide range of wettability, the proposed free-energy based method is in agreement with the direct simulation using fluid droplets. However, it is noted that for highly hydrophilic systems ($\theta < 35°$), although the contact angles obtained from the proposed method and from direct MD simulations using droplets agreed with each other within simulation uncertainty, the free-energy based method yields slightly but consistently lower contact angles compared with direct simulations. Such a difference is arguably due to the presence of a film of fluid (layering) at the solid/fluid interface when the solid/fluid attraction is strong (e.g., $\epsilon_{s,f1} = 0.9$). From Young's equation, which we used in this work to estimate the contact angle, the contact angle ($\theta$) is related to the work of adhesion ($W_a$) as

$$W_a = \gamma_{sf_2} - \gamma_{sf_1} + \gamma_{f_{1,2}} = \gamma_{f_{1,2}}(1 + \cos\theta). \quad (15)$$

However, Fernandez-Toledano *et al.*[35,55] recently found that the work of adhesion ($W_a$) may exceed the value of $\gamma_{f_{1,2}}(1+\cos\theta)$ if strong fluid layering is induced by the solid, which is consistent with the lower contact angle from the proposed method.

### B. Water/$CO_2$/silica

The contact angle of water in equilibrium with $CO_2$ on a silica Q2 surface was also studied using the proposed method. The Q2 surface of silica, which has a silanol density of 9.4 $nm^{-2}$, is highly hydrophilic and the silanol group may form hydrogen bonds with water. Similar to the LJ system with strong solid/liquid interaction, the phantom-wall method alone is not robust for the hydrophilic silica surface. It is necessary to turn the hydrophilic silica Q2 surface into a hydrophobic one, so the phantom-wall method can be applied to the hydrophobic surface to calculate the relative silica/water surface tension. Since the system studied here is polar, the interaction between silica and water is dominated by the electrostatics instead of van der Waals (VdW) interactions. While multiplying the

09 January 2024 14:51:36

scaling parameter ($\lambda$) to the energy parameter ($\epsilon$) of LJ potential reduces the silica/water vdW interactions, the electrostatic interactions between silica and water are not largely affected. Therefore, in the simulations using the BAR method, we followed Eq. (14) and tuned the size parameter ($\sigma_{Ow,Os}$) for LJ potential between oxygen of water and oxygen of silanol group, and as $\sigma_{Ow,Os}$ increased, both the LJ and electrostatic interactions decreased, which reduced the hydrophilicity of the silica surface. Similar to Figs. 4 and 5, we show the spring forces used for thermodynamic integration at different equilibrium spring lengths and the Gibbs free energy obtained with the BAR method at each intermediate $\lambda$ states, in Figs. 6 and 7. As shown in Figs. 6 and 7, the Gibbs free energy from the BAR method ($\Delta G_{BAR}$), as well as the spring force ($f_{sp}$) in the phantom-wall method, varies smoothly at each intermediate states, which indicates that the surface free energy can be obtained accurately for the silica/water system. It is noted that silica only weakly interacts with $CO_2$; therefore, the phantom-wall method can be used without any sudden transition of spring force and box length for the silica/$CO_2$ interface, as shown in Fig. S3 of the supplementary material.

From the BAR and phantom-wall methods, the contact angle of water in $CO_2$ on the silica Q2 surface is 34° ± 5° at 318 K and 145 bars, and it agrees with the contact angle calculated from the geometry of a cylindrical droplet (38° ± 4°) within simulation uncertainty. The calculated contact angle is similar to the result reported by Chen *et al.* (33° ± 4°), who calculated the contact angle from MD simulations using a cylindrical water droplet. It is noted that the molecular models for water and $CO_2$ used in this work differs from those used by Chen *et al.*;[14] however, it was found that the INTERFACE silica model yields similar interfacial properties in conjunction with several different non-polarizable water models.[46]

### C. Comparison of simulation efficiency

We have shown that the proposed method yields contact angles that are in agreement with those calculated using fluid droplets in MD simulations. In this section, we compare the efficiency of the simulations using the proposed BAR + phantom-wall methods and the simulations using cylindrical fluid droplets. We limit the comparison to the water/$CO_2$/silica system since the LJ system does not have electrostatic interactions that are present in most of the molecular models for real fluids. The one simulation that used cylindrical droplets to calculate the contact angle ran for 9 ns, and the cost was around 4600 CPU hours on an Intel Sandbridge (16 core, 2.6 GHz) processor using LAMMPS. Since a water droplet with a large radius was necessary to reduce system size effects, it was expected that the simulation would be computationally demanding although only one simulation was needed to obtain the contact angle. Additionally, the use of piston atoms in the MD simulation to regulate fluid phase pressure also increased the CPU time. For the BAR + phantom wall method, in order to calculate the relative solid/fluid surface tensions, a total of 50 simulations were performed and each simulation was 1.5 ns. In addition, another 3 sets of MD simulations were necessary to calculate the phantom wall/water, phantom wall/$CO_2$, and water/$CO_2$ surface tensions. In total, these simulations cost about 5000 CPU hours to complete on an Intel Sandbridge processor using our code. While the proposed method does not reduce the computational cost for contact angle calculations, it provides a way to predict the equilibrium contact angle without any ambiguity. Unlike the simulations of a fluid droplet, the contact angle calculated using the proposed method is not affected by the line tensions or by the Laplace pressure of the droplet since there is no curved interface present in the simulations. Moreover, the proposed method does not need to identify the interface between the fluid droplet and its surrounding fluid—it is generally difficult and subjective to identify such an interface for highly hydrophilic systems. In addition, the new method provides direct access to the surface free energy (e.g., the work of adhesion), which is an essential property for a solid/liquid system. While the droplet simulations can be used to calculate contact angles, the contact angles by themselves may not provide all the information needed to describe solid/liquid interfaces.

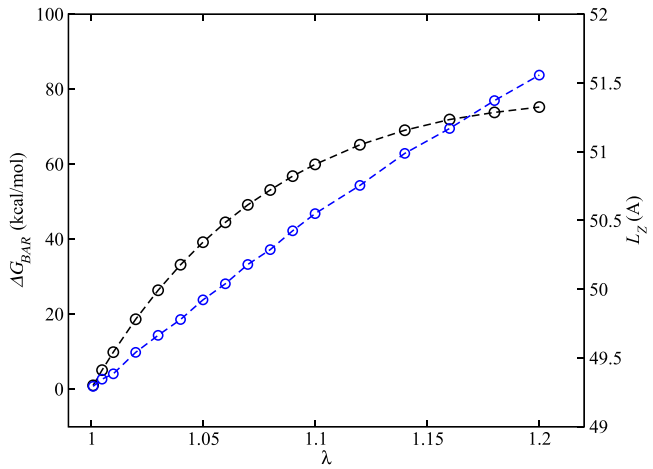


FIG. 6. Gibbs free energy (black symbols) of the end state ($\lambda$ = 1.2) and each intermediate state relative to the state of interest ($\lambda$ = 1.0) at $T$ = 318 K and $P$ = 145 bars for the water/silica system. Blue symbols are the simulation box lengths at each state. The dashed lines are a guide to the eye.

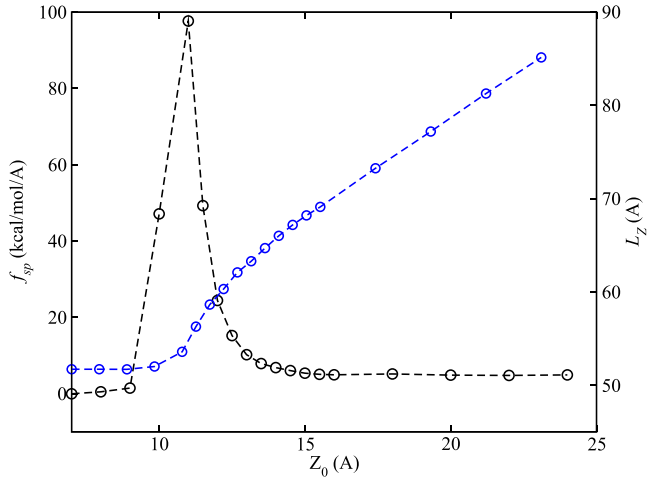


FIG. 7. Spring force ($f_{sp}$) and simulation box length ($L_z$) at different spring lengths ($Z_0$) for the water/silica system at $T$ = 318 K and $P$ = 145 bars with $\lambda$ [in Eq. (14)] equal to 1.2. Blue symbols are the simulation box lengths. The dashed lines are a guide to the eye.

09 January 2024 14:51:36

## V. CONCLUSIONS

In this work, we extended the phantom-wall method for the calculation of relative solid/fluid surface tensions to the calculation of contact angles of binary fluid mixtures on solid surfaces for both non-polar and polar systems. Using Bennett's acceptance ratio method to transform a solid/fluid interface with strong interactions to a surface with weak solid/fluid attractions, we were able to apply the phantom-wall method to obtain the relative solid/fluid surface tension without experiencing a phase transition during thermodynamic integration. The proposed method does not use any fluid droplet, and simulations can be conducted with relatively small system size. We applied the new method to a LJ solid/fluid system as well as a polar water/$CO_2$/silica system. In order to validate the new method, we also estimated the contact angles directly from the geometry of periodic cylindrical droplets in MD simulations. The contact angles obtained from the proposed method were in agreement with those obtained from simulations using cylindrical fluid droplets within simulation uncertainty for both the non-polar LJ and polar water/$CO_2$/silica systems. The computational cost of the proposed method is only slightly higher than a MD simulation that uses cylindrical fluid droplets for the water/$CO_2$/silica system. Although the computational cost is not reduced with the new method, the surface free energies can be calculated, and contact angles can be obtained without ambiguity.

Our method is similar in spirit to the calculation of a fluid/fluid surface tension from the pressure tensor anisotropy in a microscopic molecular simulation, which corresponds to the macroscopic fluid/fluid surface tension. Since no three-phase contact is present in our free energy calculation, the relative solid/fluid surface tension obtained from the proposed algorithm corresponds to its macroscopic value. Young's equation is fully valid at the macroscopic level, so the proposed algorithm provides a way to predict macroscopic contact angles from molecular force field models regardless of the validity of Young's equation at the atomic scale. It is the macroscopic contact angle that is measured in most experiments and of most interest to many scientific and industrial applications.

## SUPPLEMENTARY MATERIAL

See supplementary material for relative surface tensions, phantom wall/fluid and fluid/fluid surface tensions, examples of mole fraction distribution maps for LJ and water/$CO_2$/silica systems, and spring forces at different equilibrium spring lengths for the silica/$CO_2$ system.

## ACKNOWLEDGMENTS

Financial support for this work was provided by the Office of Basic Energy Sciences, U.S. Department of Energy, under Award No. DE-SC0002128. Additional support was provided by the National Oceanic and Atmospheric Administration (Cooperative Institute for Climate Science Award No. AWD 1004131). Calculations were performed on the Terascale Infrastructure for Groundbreaking Research in Engineering and Science (TIGRESS) computing facility at Princeton University. F.M.-P. wishes to thank A.Z.P. and his group for their great hospitality at Princeton University. This visit was supported by the Deutsche Forschungsgemeinschaft.

[1] K. L. Mittal, *Advances in Contact Angle, Wettability and Adhesion* (Wiley, 2013).
[2] T. Ingebrigtsen and S. Toxvaerd, J. Phys. Chem. C **111**, 8518 (2007).
[3] S. Becker, H. M. Urbassek, M. Horsch, and H. Hasse, Langmuir **30**, 13606 (2014).
[4] A. Malani, A. Raghavanpillai, E. B. Wysong, and G. C. Rutledge, Phys. Rev. Lett. **109**, 184501 (2012).
[5] B. Shi and V. K. Dhir, J. Chem. Phys. **130**, 034705 (2009).
[6] N. Wei, C. Lv, and Z. Xu, Langmuir **30**, 3572 (2014).
[7] F. Taherian, V. Marcon, N. F. A. van der Vegt, and F. Leroy, Langmuir **29**, 1457 (2013).
[8] T. Werder, J. H. Walther, R. L. Jaffe, T. Halicioglu, F. Noca, and P. Koumoutsakos, Nano Lett. **1**, 697 (2001).
[9] T. Koishi, K. Yasuoka, S. Fujikawa, and X. C. Zeng, ACS Nano **9**, 6834 (2011).
[10] F. Jiménez-Ángeles and A. Firoozabadi, J. Phys. Chem. C **120**, 11910 (2016).
[11] G. Javanbakht, M. Sedghi, W. Welch, and L. Goual , Langmuir **31**, 5812 (2015).
[12] S. Tsuji, Y. Liang, M. Kunieda, S. Takahashi, and T. Matsuoka, Energy Procedia **37**, 5435 (2013).
[13] C. M. Tenney and R. T. Cygan, Environ. Sci. Technol. **48**, 2035 (2014).
[14] C. Chen, B. Dong, N. Zhang, W. Li, and Y. Song, Energy Fuels **30**, 5027 (2016).
[15] L. Schimmele, M. Napiorkowski, and S. Dietrich, J. Chem. Phys. **127**, 164715 (2007).
[16] J. Zhang, F. Leroy, and F. Müller-Plathe, Phys. Rev. Lett. **113**, 046101 (2014).
[17] G. Scocchi, D. Sergi, C. D'Angelo, and A. Ortona, Phys. Rev. E **84**, 061602 (2011).
[18] G. J. Gloor, G. Jackson, F. J. Blas, and E. de Miguel, J. Chem. Phys. **123**, 134703 (2005).
[19] R. Bahadur, L. M. Russell, and S. Alavi, J. Phys. Chem. B **111**, 11989 (2007).
[20] F. Leroy and F. Müller-Plathe, J. Chem. Phys. **133**, 044110 (2010).
[21] F. Leroy, D. J. V. A. dos Santos, and F. Müller-Plathe, Macromol. Rapid Commun. **30**, 864 (2009).
[22] F. Leroy and F. Müller-Plathe, Langmuir **31**, 8335 (2015).
[23] F. Leroy, S. Liu, and J. Zhang, J. Phys. Chem. C **119**, 28470 (2015).
[24] F. Leroy, J. Chem. Phys. **145**, 164705 (2016.
[25] E. M. Grzelak and J. R. Errington, J. Chem. Phys. **128**, 014710 (2008).
[26] E. M. Grzelak and J. R. Errington, J. Chem. Phys. **132**, 224702 (2010).
[27] V. Kumar and J. R. Errington, Mol. Simul. **39**, 1143 (2013).
[28] V. Kumar and J. R. Errington, J. Phys. Chem. C **117**, 23017 (2013).
[29] M. Kanduc and R. R. Netz, J. Chem. Phys. **146**, 164705 (2017).
[30] M. Kanduc and R. R. Netz, Proc. Natl. Acad. Sci. U. S. A. **112**, 12338 (2015).
[31] S. Iglauer, Acc. Chem. Res. **50**, 1134 (2017).
[32] S. Saville, J. Chem. Soc., Faraday Trans. 2 **73**, 1122 (1977).
[33] D. Seveno, T. D. Blake, and J. De Coninck, Phys. Rev. Lett. **111**, 096101 (2013).
[34] S. K. Das and K. Binder, Europhys. Lett. **92**, 26006 (2010).
[35] J-C. Fernandez-Toledano, T. D. Blake, and J. De Coninck, Langmuir **33**, 2929 (2017).
[36] C. H. Bennett, J. Comput. Phys. **22**, 245 (1976).
[37] I. C. Bourg, L. E. Beckingham, and D. J. DePaolo, Environ. Sci. Technol. **49**, 10265 (2015).
[38] J. G. Kirkwood and F. P. Buff, J. Chem. Phys. **17**, 338 (1949).
[39] A. R. Nair and S. P. Sathian, J. Chem. Phys. **137**, 084702 (2012).
[40] Q. Broughton and G. H. Gilmer, J. Chem. Phys. **84**, 5759 (1986).
[41] R. L. Davidchack and B. B. Laird, J. Chem. Phys. **118**, 7651 (2003).
[42] X. Qi, Y. Zhou, and K. A. Fichthorn, J. Chem. Phys. **145**, 194108 (2016).
[43] J. R. Espinosa, C. Vega, and E. Sanz, J. Chem. Phys. **141**, 134709 (2014).
[44] T. Schneider and E. Stoll, Phys. Rev. B **17**, 1302 (1978).
[45] M. Parrinello and A. Rahman, J. Appl. Phys. **52**, 7182 (1981).

09 January 2024 14:51:36

[46]F. S. Emami, V. Puddu, R. J. Berry, V. Varshney, S. V. Patwardhan, C. C. Perry, and H. Heinz, Chem. Mater. **26**, 2647 (2014).
[47]H. J. C. Berendsen, J. R. Grigera, and T. P. Straatsma, J. Phys. Chem. **91**, 6269 (1987).
[48]J. G. Harris and K. H. Yung, J. Phys. Chem. **99**, 12021 (1995).
[49]H. Jiang, I. G. Economou, and A. Z. Panagiotopoulos, Acc. Chem. Res. **50**, 751 (2017).
[50]H. Jiang, I. G. Economou, and A. Z. Panagiotopoulos, J. Phys. Chem. B **121**, 1386 (2017).
[51]D. Frenkel and B. Smit, *Understanding Molecular Simulation From Algorithms to Applications* (Academic Press, Inc., Orlando, FL, USA, 2001).
[52]I. Yeh and M. L. Berkowitz, J. Chem. Phys. **111**, 3155 (1999).
[53]J. P. Ryckaert, G. Ciccotti, and H. J. C. Berendsen, J. Comput. Phys. **23**, 327 (1977).
[54]S. Plimpton, J. Comput. Phys. **117**, 1 (1995).
[55]J.-C. Fernandez-Toledano, T. D. Blake, P. Lambert, and J. De Coninck, Adv. Colloid Interface Sci. **245**, 102 (2017).

09 January 2024 14:51:36